Langmuir

Article

pubs.acs.org/Langmuir

Tetrathiafulvalene Terminal-Decorated PAMAM Dendrimers for Triggered Release Synergistically Stimulated by Redox and CB[7]

Xiaohui Zhang,[†] Yi Zeng,*[,†] Tianjun Yu,[†] Jinping Chen,[†] Guoqiang Yang,*[,‡] and Yi Li*[,†]

[†]Key Laboratory of Photochemical Conversion and Optoelectronic Materials, Technical Institute of Physics and Chemistry, Chinese Academy of Sciences, Beijing 100190, People's Republic of China

[‡]Beijing National Laboratory for Molecular Sciences (BNLMS), Key Laboratory of Photochemistry, Institute of Chemistry, Chinese Academy of Sciences, Beijing 100190, People's Republic of China

Supporting Information

ABSTRACT: A series of polyamidoamine (PAMAM) dendrimers with tetrathiafulvalene (TTF) at the periphery (G*n*-PAMAM-TTF), generation 0−2, were synthesized. These functionalized dendrimers exist as nanospheres with diameters around 80−100 nm in aqueous phase, which can encapsulate hydrophobic molecules. The terminal TTF groups can go through a reversible redox process upon addition of the oxidizing and reducing agents. Each terminal $TTF^{+\bullet}$ group of the oxidized G*n*-PAMAM-TTF assembled with cucurbit[7]uril (CB[7]) forming a 1:1 inclusion complex with association constants of $(3.14 \pm 0.36) \times 10^5$, $(1.29 \pm 0.12) \times 10^6$, and $(1.79 \pm 0.24) \times 10^6$ M^{-1} for generation 0−2, respectively, even at the aggregate state. The formation of the inclusion complex loosened the structure of the nanospheres and initiated the release of cargo, and the release mechanism was validated by dynamic light scattering (DLS), cryo-transmission electron microscopy (TEM), and electron paramagnetic resonance (EPR) experiments. This study provides a potential strategy for the development of drug delivery systems synergistically triggered by redox and supramolecular assembly.

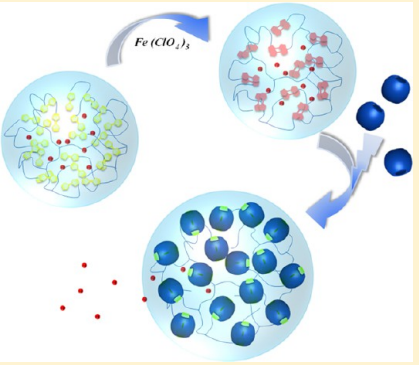

INTRODUCTION

For decades, great efforts have been devoted to the development of supramolecular systems for various applications, among which drug delivery is one of the most attractive fields.[1,2] Compared with the conventional drug carriers, the drug delivery systems with stimulus-responsive properties have received more attention because of their improved therapeutic activity. Therefore, various kinds of inorganic and organic assemblies capable of encapsulation and triggered release in response to stimuli, such as pH,[3−7] temperature,[8−11] enzyme,[12−15] redox,[16−21] and light,[22−29] have been developed. Incorporated with the external stimuli, the supramolecular interactions, especially the host−guest interactions, have been employed to construct more complex and smart delivery systems. Upon external stimuli, the supramolecular architectures were assembled/disassembled, or the formed supramolecular nanovalves were activated; consequently, the encapsulated cargo was released.[4,30−34]

Dendrimers, which have unique characteristics including monodispersity, modifiable surface functionality, and defined nanoscopic size and structure, have been extensively studied as carriers in drug delivery applications.[35−38] Polyamidoamine (PAMAM) dendrimers have shown promise in drug delivery owing to their water solubility, high drug-loading ability, and biocompatibility.[39−41] Tetrathiafulvalene (TTF) is a nonaromatic 14π-electron donor and can be reversibly transformed to the cation radical ($TTF^{+\bullet}$) and dication (TTF^{2+}) by either chemical or electrochemical oxidation at easily accessible potentials.[42−45] The specific redox characteristics of TTF make it and its derivatives applied in supramolecular chemistry extensively. The cationic $TTF^{+\bullet}$ can be encapsulated and stabilized in the cavity of cucurbiturils,[46,47] forming a 1:1 inclusion complex with cucurbit[7]uril (CB[7]). The association and dissociation of the inclusion complexes can be reversibly tuned by redox-stimulus[46−48] because of their reversible two successive one-electron oxidation processes by either chemical or electrochemical oxidation. On the basis of the redox function of TTF and the assembly with CB[7], a smart release system triggered by synergetic stimuli of oxidation and supramolecular interaction can be developed.

In the present work, we synthesized a series of PAMAM dendrimers with TTF groups covalently modified at the periphery. These dendrimers exist as nanospheres in aqueous phase, which can encapsulate hydrophobic guest molecules. The TTF moieties within the nanosphere can be oxidized and reduced reversibly. Upon the redox stimulus, the terminal TTF groups transform to the oxidized form $TTF^{+\bullet}$, which further interact with CB[7] forming pseudorotaxane at the periphery of dendrimers. The formation of the pseudorotaxane loosens the

Received: November 12, 2013
Revised: December 24, 2013
Published: December 27, 2013

Scheme 1. Structure of the G*n*-PAMAM-TTF (n = 0−2) Dendrimers

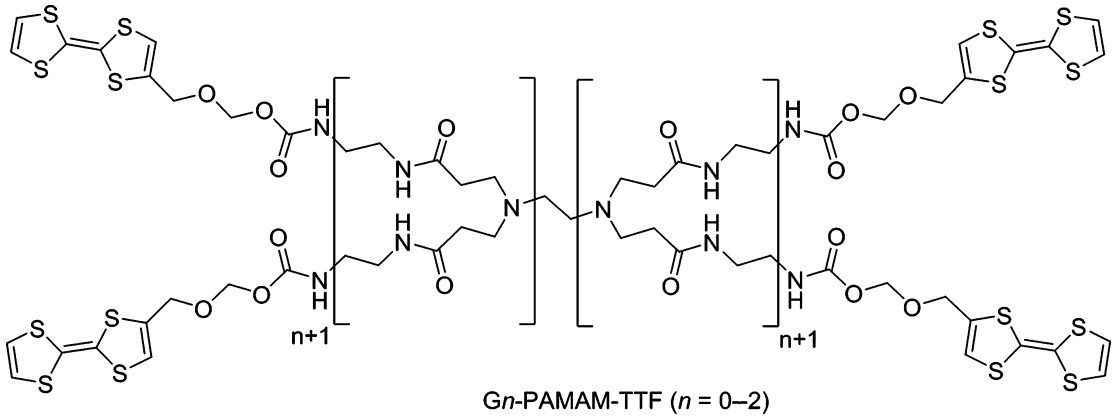

Scheme 2. Structure of Model and the Formation of Inclusion Complex between Model and CB[7] upon the Redox Stimulus

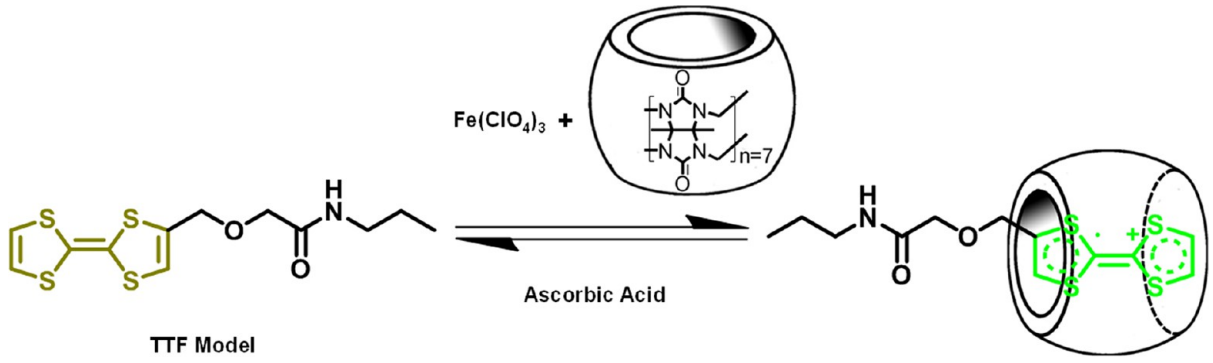

structure of the nanospheres and initiates the release of cargo, making the triggered release achieved.

RESULTS AND DISCUSSION

Preparation of TTF Terminated PAMAM Dendrimers, Model, and Aqueous Nanoparticle Dispersions of Dendrimers. PAMAM dendrimer was chosen as the scaffold of the drug carrier because of its convenient synthesis and promise performance in drug delivery studies. The TTF terminated PAMAM dendrimers G*n*-PAMAM-TTF (n = 0−2, Scheme 1) were obtained by an efficient reaction of the terminal amino groups of PAMAM dendrimer with succinimido-*N*-(4-tetrathiafulvalenylmethoxyl) acetate. The functionalization extents of the periphery amino groups for generations 0−2 were all 100% according to their ^{1}H NMR spectra. The structure of G*n*-PAMAM-TTF (n = 0−2) was characterized by means of ^{1}H NMR spectra, matrix-assisted laser desorption ionization time-of-flight (MALDI−TOF) mass spectrometry, and IR spectra (see the Supporting Information). These dendrimers were found insoluble in water and common organic solvents such as hexane, CH_2Cl_2, tetrahydrofuran (THF), and dimethylformamide (DMF) except in dimethyl sulfoxide (DMSO). The poor solubility of G*n*-PAMAM-TTF may be attributed to the large amount of hydrophobic TTF units at the periphery of dendrimers and the hydrogen bonding among the PAMAM backbones. The model compound ((4-tetrathiafulvalenylmethoxyl)-*N*-propylacetamide, Model, Scheme 2) was directly synthesized by the condensation of (4-tetrathiafulvalenylmethoxyl) acetic acid with propylamine in the presence of EDC (1-ethyl-3-(3-dimethylaminopropyl) carbodiimide) and HOBt (1-hydroxybenzotriazole). Model is well soluble in most organic solvents and can be dissolved in DMSO-H_2O (1:100, v/v) with moderate solubility.

The dispersions of G*n*-PAMAM-TTF were prepared by shaking (hand shaking with a frequency of two to three times per second) the mixture of a certain amount of DMSO solution of G*n*-PAMAM-TTF and water (DMSO:H_2O = 1:100, v/v) for 30 s at ambient temperature, and the samples were placed for ∼5 min before further measurements. The dispersions of G*n*-PAMAM-TTF are optically transparent for the naked-eye observation but show tiny light dispersion in the absorption spectra. The formation of aggregates was confirmed by dynamic light scattering (DLS) experiment results, which gave the hydrodynamic diameters to be approximately 80−100 nm (Figures S19−S21 of the Supporting Information) for generations 0−2. Cryo-transmission electron microscopy (cryo-TEM) images were further used to characterize the morphology of the aggregates, which demonstrated that the aggregates derived from G*n*-PAMAM-TTF are spherical. The dispersions of aggregates were prepared several times, and the similar results of their DLS data indicated that the preparation method in our experiments is reproducible.

Reversible Redox-Induced Noncovalent Modification of the G*n*-PAMAM-TTF Systems. CB[7], one member of the cucurbit[*m*]uril family (CB[*m*], m = 5−10),[49−51] is used as the host molecule. The cucurbit[*m*]uril family, a series of synthetic macrocyclic compounds, consists of numbers of glycoluril units linked by methylene bridges. The rigid hydrophobic cavity and oxygen atoms of the glycoluril carbonyl located along the edges endow cucurbiturils specific self-assembly properties with cationic guests through the hydrophobic and ion−dipole interactions.[49−53] Because CB[7] has a suitable hydrophobic

dx.doi.org/10.1021/la404349w | *Langmuir* 2014, 30, 718−726

cavity to encapsulate the TTF group, it is expected that CB[7] can form a 1:1 inclusion complex with each terminal cation radical $TTF^{+\bullet}$ of the oxidized G*n*-PAMAM-TTF with high affinity.[46,47]

In the present work, $Fe(ClO_4)_3$ and ascorbic acid are chosen as the oxidant and the reductant to accomplish the reversible redox processes of TTF groups chemically. The reversible redox transformation between TTF and $TTF^{+\bullet}$ was illustrated by absorption spectra upon addition of $Fe(ClO_4)_3$ and ascorbic acid to the solution of Model in DMSO-H_2O (1:100, v/v). Upon addition of 1 equivalent $Fe(ClO_4)_3$, the absorption band with maximum at 330 nm assigned to the TTF vanishes and several new absorption bands with maxima at 380, 430, and 590 nm dominate the whole spectrum, which can be assigned to the TTF cation radical ($TTF^{+\bullet}$),[46,54] indicative of a complete oxidation of TTF to $TTF^{+\bullet}$ (Figure S5 of the Supporting Information). Moreover, the absorption spectrum of TTF can be restored instantly after addition of the reducing agent ascorbic acid. The color of the Model solution changes from light yellow to green during the oxidation process and back to light yellow after addition of ascorbic acid.

The oxidation processes of G*n*-PAMAM-TTF were monitored by the UV spectra. When 3 equivalent $Fe(ClO_4)_3$ was added to the dispersions of G*n*-PAMAM-TTF (n = 0–2) in DMSO-H_2O (1:100, v/v), the color of the dispersions changed from light yellow to green at the beginning and then to pink in a few seconds, unlike the color of Model which stopped at the step of green. The UV–vis spectra of the oxidized G*n*-PAMAM-TTF are completely different from G*n*-PAMAM-TTF and the oxidized Model (G2-PAMAM-TTF as an example shown in Figure 1). After addition of sufficient $Fe(ClO_4)_3$ to

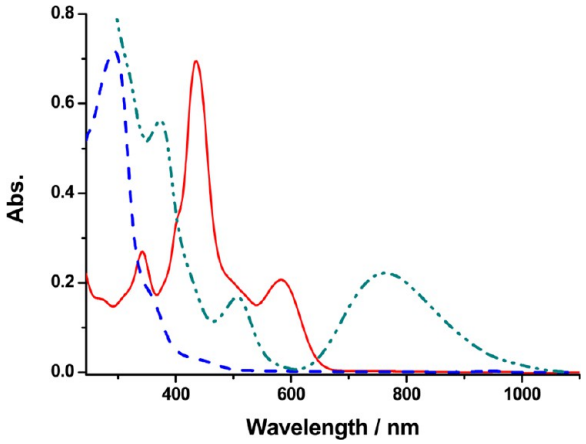

Figure 1. Absorption spectra of the oxidized Model (4.1×10^{-5} M) (red solid line), G2PAMAM-TTF ([TTF] = 4.1×10^{-5} M) (blue dash line), and the oxidized G2PAMAM-TTF ([TTF] = 4.1×10^{-5} M) (green dash dot line) in DMSO-H_2O (1:100, v/v).

the dispersion of G*n*-PAMAM-TTF, the absorption spectra with maxima at 490, 520, and 790 nm were detected for G*n*-PAMAM-TTF of generations 0–2, which can be characterized as the TTF cation radical dimer (TTF_2^{2+}).[44–46] No TTF_2^{2+} formation was observed in the solution of Model, which can be ascribed to the better solubility of Model. In contrast, the adjacent $TTF^{+\bullet}$ groups within nanoparticles can proceed the intramolecular and intermolecular dimerization to form TTF_2^{2+}. No significant difference was observed for three generations of dendrimers. Combining the observation of the color change and the absorption spectra, the oxidation process of G*n*-PAMAM-TTF can be described as follows: the periphery TTF groups are first oxidized to the cation radicals, and then the intra- or internanoparticle oxidized TTF groups dimerize to TTF_2^{2+}. Similar as Model, the addition of an excess amount of ascorbic acid restores the absorption spectra to that of TTF rapidly, indicative of a reversible redox process even at the aggregate state.

To understand the binding affinity of $TTF^{+\bullet}$ toward CB[7], the absorption titration experiment of the oxidized Model (completely oxidized by $Fe(ClO_4)_3$) with CB[7] was carried out. As shown in Figure 2, the absorption spectra of the

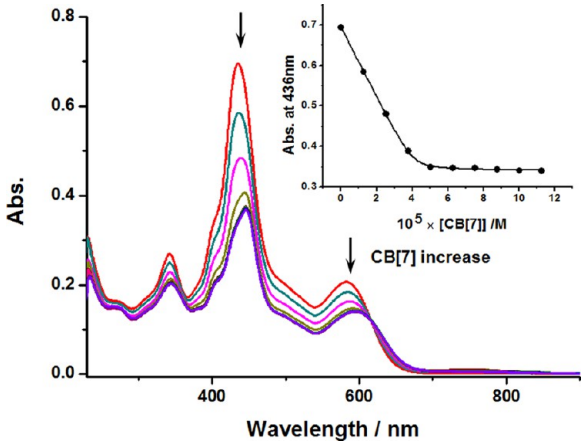

Figure 2. Absorption spectra of the oxidized Model (4.1×10^{-5} M, DMSO/H_2O = 1/100, v/v) upon titration with CB[7] (0–2.7 equiv). Inset: Plot of absorbance at 436 nm as a function of CB[7] concentration, and the solid line represents the best fit of the data to a 1:1 binding mode.

oxidized Model show an evident drop and a slightly bathochromic shift with addition of CB[7]. The inset shows a plot of the absorbance at 436 nm as a function of the concentration of CB[7], and the optimum fit of the data gives a 1:1 binding model with association constant $K_a = (2.36 \pm 0.23) \times 10^6$ M^{-1}. Obviously, CB[7] and the oxidized Model can form a stable inclusion complex with a 1:1 binding mode (Scheme 2). Upon addition of excess ascorbic acid into the solution of the inclusion complex sequentially, an evident decrease of the $TTF^{+\bullet}$ absorption within the region of 300–770 nm was observed, and the spectrum was dominated by the absorption band of TTF with maximum at 330 nm (Figure S6 of the Supporting Information). This result indicates that the TTF cation radical was reduced. The reduction process took a few hours, which is much slower than the case in the absence of CB[7] (a few seconds).

The details of the complexation between the oxidized G*n*-PAMAM-TTF and CB[7] were also investigated by the UV–vis titration experiments. Upon addition of CB[7] to the oxidized G*n*-PAMAM-TTF dispersion, the lower energy absorption band of TTF_2^{2+} with maximum at 790 nm decreases, which is accompanied by the formation of new absorption bands with maxima at 442 and 600 nm assigned to $TTF^{+\bullet}$. The UV–vis spectra of the oxidized G*n*-PAMAM-TTF reach an invariable stage when the addition amount of CB[7] is up to 1 equivalent based on the terminal TTF group (G2-PAMAM-TTF as a representative example shown in Figure 3a), indicative of the formation of a 1:1 inclusion complex between

dx.doi.org/10.1021/la404349w | *Langmuir* 2014, 30, 718–726

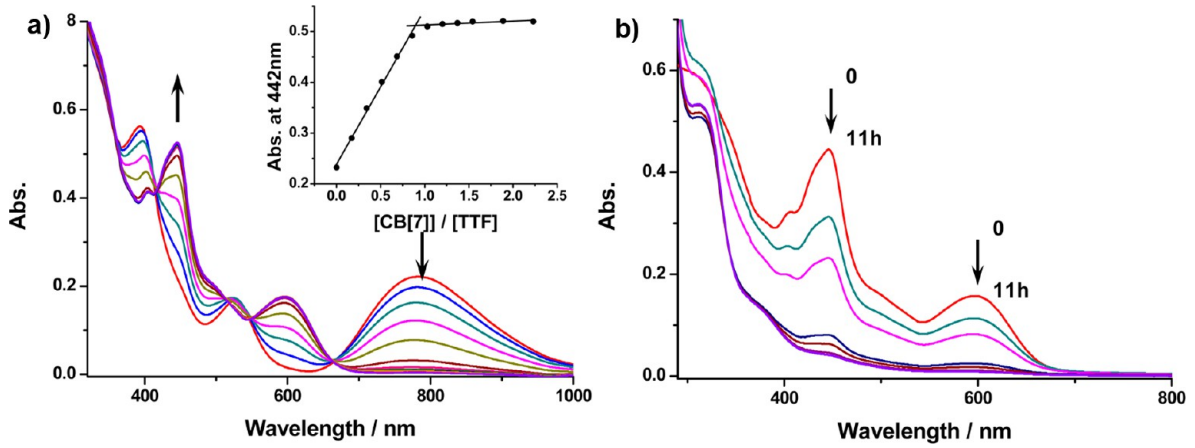

Figure 3. (a) Absorption spectra of the oxidized G2-PAMAM-TTF ([TTF] = 4.1×10^{-5} M, DMSO:H_2O = 1:100, v/v) during addition of CB[7] (0–2.3 equiv). Inset: Plots of absorbance (442 nm) as a function of [CB[7]]/[TTF], which reveals a 1:1 binding stoichiometry. (b) Absorption spectra of the inclusion complex of the oxidized G2-PAMAM-TTF and CB[7] at different reduction times after addition of excess ascorbic acid ([TTF] = [CB[7]] = 3.7×10^{-5} M, DMSO:H_2O = 1:100, v/v).

each $TTF^{+\bullet}$ group and CB[7]. Spectrum changes were fitted by approximately taking the terminal $TTF^{+\bullet}$ group as an individual guest to CB[7], giving K_a = $(3.14 \pm 0.36) \times 10^5$, $(1.29 \pm 0.12) \times 10^6$, and $(1.79 \pm 0.24) \times 10^6$ M^{-1} for generations 0–2, respectively (Figure S7 of the Supporting Information). Obviously, the cation radical dimer is dissociated by the formation of the inclusion complexes between the terminal TTF cation radicals and CB[7]. The formation of the inclusion complexes between the terminal $TTF^{+\bullet}$ and CB[7] was also confirmed by the MALDI-TOF spectra (Figures S9 and S10 of the Supporting Information). The electron paramagnetic resonance (EPR) experiments further strengthened the transformation between TTF_2^{2+} and $TTF^{+\bullet}$ (Figure 4 and Figures

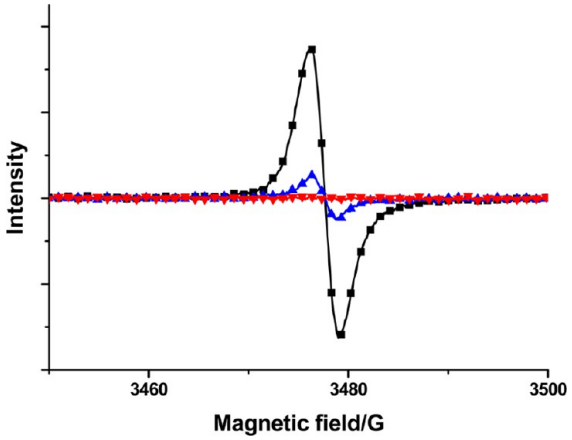

Figure 4. EPR spectra of G0-PAMAM-TTF (▼), the oxidized G0-PAMAM-TTF (▲), and the inclusion complex of the oxidized G0-PAMAM-TTF with CB[7] (■) ([TTF] = [CB[7]] = 1.0×10^{-4} M, DMSO:H_2O = 1:100, v/v) at ambient conditions.

S11 and S12 of the Supporting Information). In the absence of CB[7], the oxidized G*n*-PAMAM-TTF (*n* = 0–2) show very weak EPR signals which can be attributed to the incomplete dimerized $TTF^{+\bullet}$. Upon addition of CB[7], the EPR signal becomes much stronger, indicative of an increased amount of $TTF^{+\bullet}$, which must be transformed from the dissociation of TTF_2^{2+}. Unfortunately, the lower solubility of G*n*-PAMAM-TTF in aqueous medium could not afford the NMR measurement. Further addition of ascorbic acid to the dispersions of the inclusion complex of the oxidized G*n*-PAMAM-TTF (*n* = 0–2) and CB[7] made the absorption spectra gradually approach those of G*n*-PAMAM-TTF as the Model system did, suggesting that $TTF^{+\bullet}$ was reduced to regenerate G*n*-PAMAM-TTF (Figure 3b and Figure S8 of the Supporting Information). These results reveal that the transformation between TTF and $TTF^{+\bullet}$ (TTF_2^{2+}) within the G*n*-PAMAM-TTF nanospheres is a reversible process. The reduction process of $TTF^{+\bullet}$ embedded in CB[7] for either Model or dendritic systems needs several hours, which is much slower than that of the unassociated $TTF^{+\bullet}$, indicative of an enhanced stabilization of $TTF^{+\bullet}$ by encapsulation within CB[7].

Triggered Release from the Redox-Induced Formation of Supramolecular Assembly. G2-PAMAM-TTF was chosen as the carrier because of its bulky dendritic backbone capable of encapsulation of more cargoes. The supramolecular assembly triggered release of a hydrophobic payload from the nanospheres of G2-PAMAM-TTF was assessed by using Nile Red (NR) as a model payload. The NR-loaded nanospheres were prepared by following the same procedure for preparation of the dispersion of G2-PAMAM-TTF using a mixture of NR and G2-PAMAM-TTF with a mole ratio [NR]/[G2-PAMAM-TTF] of 0.5 instead of the neat G2-PAMAM-TTF. The encapsulation of NR within the nanospheres derived from G2-PAMAM-TTF was confirmed by strong emission of NR with maximum at 656 nm in the nanosphere dispersion because NR was emissive in hydrophobic environment but nonemissive in water.

The release process of NR from the nanospheres of G2-PAMAM-TTF was studied by monitoring the emission of NR in the nanosphere dispersion with excitation at 580 nm. Without applying trigger, the nanosphere is stable in solution (Figure S14 of the Supporting Information), and thus, premature release of cargoes is prevented. Addition of 3 equivalent $Fe(ClO_4)_3$ based on the terminal TTF groups to the NR-loaded nanosphere dispersion resulted in no change of the emission intensity of this dispersion, which indicated that the oxidation of the terminal TTF groups of G2-PAMAM-TTF could not initiate the release of the entrapped NR (Figure S15 of the Supporting Information). Upon further addition of 1

dx.doi.org/10.1021/la404349w | *Langmuir* 2014, 30, 718–726

equivalent CB[7] based on the terminal TTF groups to the oxidized NR-loaded nanosphere dispersion, the encapsulated NR was released gradually from the nanospheres (Figure S16 of the Supporting Information). The supramolecular assembly triggered-release profile of the oxidized nanosphere dispersion in the presence of CB[7] and those of two control samples (leakage from the neutral nanosphere dispersion and the oxidized nanosphere dispersion in the absence of CB[7]) are summarized in Figure 5. The spectroscopic results illustrate

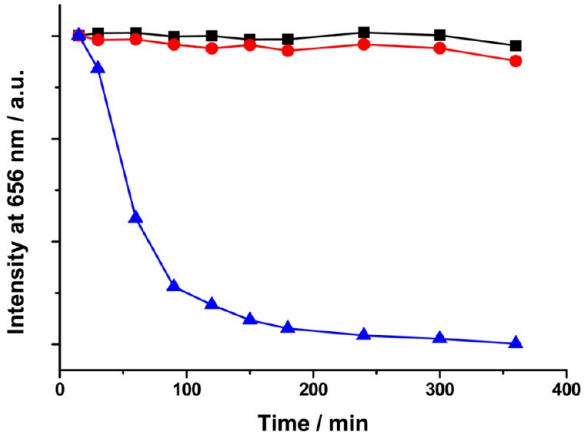

Figure 5. Release profiles of NR from the oxidized nanospheres in the presence of CB[7] (▲) and in the absence of CB[7] (●) and from the neutral nanospheres (■) in DMSO-H_2O ([G2-PAMAM-TTF] = 1.0×10^{-5} M, DMSO/H_2O = 1/100, v/v).

that the oxidation transformed the hydrophobic terminal TTF groups to the cation radical form $TTF^{+\bullet}$ but further dimerized to TTF_2^{2+} rapidly. Because one nanosphere consists of numerous molecules of G2-PAMAM-TTF, the dimerization between two $TTF^{+\bullet}$ can occur intra- and intermolecularly. Although the oxidation of G2-PAMAM-TTF increases the hydrophilicity of the nanospheres, the intermolecular dimerization of $TTF^{+\bullet}$ cross-links the G2-PAMAM-TTF molecules within the nanosphere, making nanospheres shape-persistent (see the cryo-TEM images below) and guest molecules sequestered. To exclude the effect of the direct interaction between NR and CB[7] on the release, the binding constant between NR and CB[7] was examined. The emission titration experiments show that NR and CB[7] form a 1:1 complex with a binding constant of $(2.48 \pm 0.28) \times 10^3$ M^{-1} in DMSO-H_2O (1/100, v/v) (Figure S13 of the Supporting Information). The binding constant of NR with CB[7] is about three magnitudes lower than those of the terminal oxidized TTF groups of G*n*-PAMAM-TTF with CB[7], which demonstrates that the additive CB[7] preferentially forms the inclusion complex with $TTF^{+\bullet}$. Taking account of the release results and the characteristics of the redox controlled noncovalent modification of the G2-PAMAM-TTF, we infer that the formation of the pseudorotaxane between the terminal oxidized TTF groups of G2-PAMAM-TTF and CB[7] triggered the release. Because the aqueous dispersion of NR is unstable, the fluorescence behavior of NR in the absence of G2-PAMAM-TTF could not be measured accurately. Thus, the control experiments on the fluorescence of NR were carried out by using Tween-80 instead of G2-PAMAM-TTF. Upon addition of $Fe(ClO_4)_3$ and further addition of CB[7], no significant change of the fluorescence intensity of NR was observed within 240 min, which validated the reality of the triggered release of entrapped NR from the nanospheres of G2-PAMAM-TTF (Figures S24 and S25 of the Supporting Information). How does the formation of pseudorotaxanes stimulate the release of NR from the nanospheres? The release caused by the dissociation of nanospheres was first considered because the formation of pseudorotaxanes de-cross-links the cross-linkages within the nanospheres. If the nanospheres were disaggregated, the release of NR should be a burst process, which is obviously contrary to the experiment results. The structure change of the nanospheres was further considered to be the cause of the NR release. The formation of the pseudorotaxanes did not endow the dendrimer molecule enough hydrophilicity to dissolve in aqueous phase and only expanded the dendritic backbone which loosened the structure of the nanospheres; consequently, the encapsulated NR was released gradually from the pseudorotaxane-formed nanospheres. The proposed release mechanism was validated by the DLS and cryo-TEM experiment results.

The morphology and the size of the nanospheres derived from G2-PAMAM-TTF after the oxidation and supramolecular assembling processes were measured by the cryo-TEM and

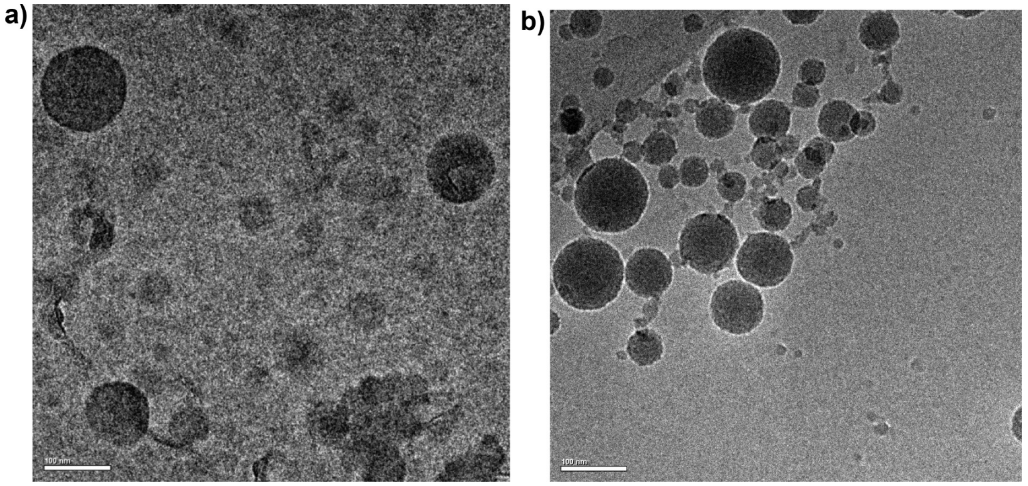

Figure 6. Cryo-TEM images of (a) the nanospheres derived from G2-PAMAM-TTF and (b) the inclusion complex of the oxidized G2-PAMAM-TTF with CB[7] . Scale bar represents 100 nm.

dx.doi.org/10.1021/la404349w | *Langmuir* 2014, 30, 718−726

Scheme 3. Visual Expression of the Release Process by the Redox-Induced Supramolecular Stimulus

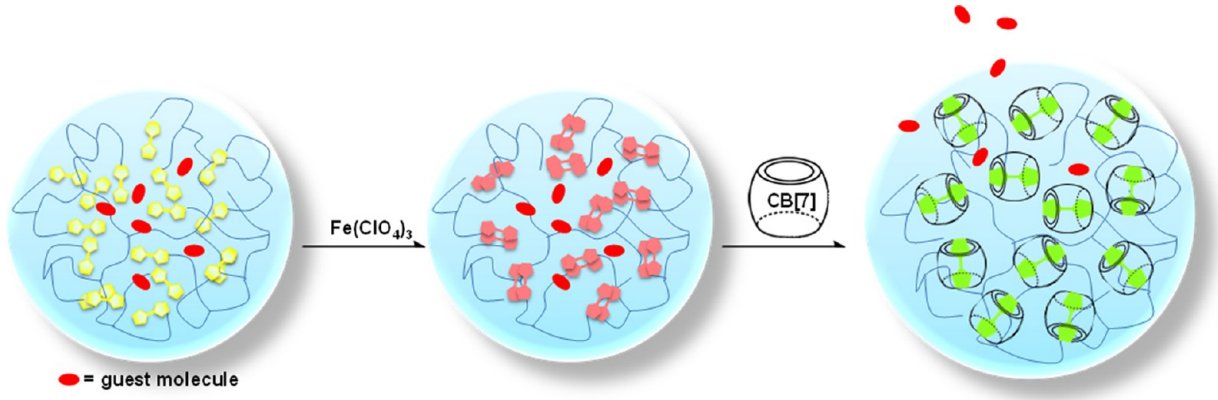

DLS experiments. The cryo-TEM images reveal that the spherical shape of the aggregates persists after oxidation and even after further assembling with CB[7] (Figure 6 and Figures S17 and S18 of the Supporting Information). The DLS data demonstrate that the hydrodynamic diameters of the nanospheres of G2-PAMAM-TTF before and after oxidation process are 82 and 79 nm with polydispersity indices (PDI) of 0.15 and 0.17, respectively (Figures S21 and S22 of the Supporting Information). However, its hydrodynamic diameter increases dramatically after assembling with CB[7], giving the number to be 106 nm (Figure S23 of the Supporting Information). The cryo-TEM images and the results of the size change for the nanospheres of G2-PAMAM-TTF obtained by DLS validate the proposed release mechanism. The formation of the pseudorotaxanes loosens the structure of nanospheres, which triggers the release of the entrapped cargo. Considering the polydisperse aggregates, the release rate of NR from the nanospheres of G2-PAMAM-TTF may be affected by the size of nanospheres. The release profile of NR represents an average result from nanospheres with different sizes. The visual expression of the release process is illustrated in Scheme 3. During the oxidation process, the terminal TTF groups are converted into their oxidized form $TTF^{+\bullet}$ and the intermolecular dimerization of $TTF^{+\bullet}$ cross-links the nanosphere, which keeps the guest molecules in sequestration. When 1 equivalent CB[7] based on the terminal TTF groups is added to the oxidized NR-loaded nanosphere dispersion, each oxidized terminal $TTF^{+\bullet}$ group threads into the cavity of CB[7] forming a pseudorotaxane, which loosens the structure of the nanospheres, and NR is released gradually.

CONCLUSION

Supramolecular interactions have attracted much attention because of their advantages such as reversibility, selectivity, and tunability. The stimulus-responsive supramolecular interactions have shown potential in smart drug delivery systems. In this work, we designed and synthesized a series of redox active dendrimers G*n*-PAMAM-TTF (n = 0−2), which form 80−100 nm nanospheres in aqueous phase, and the hydrophobic guest molecules can be encapsulated within nanospheres. The terminal TTF groups are easily oxidized to $TTF^{+\bullet}$, which further go through the intra- and intermolecular dimerization to form TTF_2^{2+}, thus stabilizing the nanospheres and keeping the encapsulated guest molecules sequestered. In the presence of one equivalent CB[7] based on the terminal TTF, TTF_2^{2+} disassociates and each oxidized terminal TTF group is encapsulated into CB[7] to form the well-defined pseudorotaxane assemblies even within nanospheres. The redox-triggered formation of the pseudorotaxane assemblies expands the structure of nanospheres and triggers the release of the entrapped cargo. The present study provides a potential strategy for developing drug delivery systems synergistically triggered by redox and supramolecular assembly.

EXPERIMENTAL SECTION

Methods. IR spectra were obtained on a Varian Excalibur 3100 spectrometer. ^{1}H NMR (400 MHz) spectra were performed on a Bruker Avance Π-400 spectrometer. MALDI-TOF and electrospray ionization (ESI) mass spectra were carried out on a Bruker MicroFlex mass spectrometer and a Waters LCT Premier XE apparatus, respectively. Milli-Q water (18.2 MΩ·cm) was prepared by Milli-Q Integral Ultrapure Water Production Unit. UV/vis absorption spectra were recorded by using a Shimadzu UV-1601PC spectrometer. Fluorescence measurements were performed on a Hitachi F-4500 spectrometer with optical path of 1 cm. Dynamic light scattering measurements were performed on a Malvern Zetasizer Nano ZS90. The cryo-TEM images were obtained by a Tecnai 20 transmission electron microscope. Orbital rotation was carried out on a WSZ-50A orbital shaker. The EPR spectra were obtained on an ESP300E spectrometer.

Materials. Reagents were purchased from Acros, Alfa Aesar, or Bejing Chemical Works and were used without further purification unless otherwise noted. Milli-Q water was used in aqueous experiments.

Synthesis and Characterization of the Compounds. Tetrathiafulvalene and (4-tetrathiafulvalenylmethoxyl) acetic acid were synthesized according to the literature.[55−58]

Succinimido-N-(4-tetrathiafulvalenylmethoxyl) Acetate. (4-Tetrathiafulvalenylmethoxyl) acetic acid (100 mg, 0.34 mmol) and *N*-hydroxy succinimide (47 mg, 0.41 mmol) were dissolved in 10 mL of dry THF. 1-Ethyl-(3-dimethylaminopropyl) carbodiimde hydrochloride (EDC) (85 mg, 0.44 mmol) was added. The dark yellow solution was stirred under nitrogen at room temperature overnight. After that, the solvent was removed under vacuum. The residue was dissolved in CH_2Cl_2, was washed with water (three times), and then was dried with Mg_2SO_4. After evaporation of the solvent, the crude product was purified by column chromatography on silica gel (CH_2Cl_2/CH_3OH, 15/1, v/v) to give the product (110 mg, 85%) as a yellow solid. ^{1}H NMR (DMSO-d_6): δ = 6.78 (s, 1H), 6.72 (s, 2H), 4.62 (s, −O**C**$\mathbf{H_2}$−, 2H), 4.41 (s, TTF**C**$\mathbf{H_2}$−, 2H), 2.84 (s, 4H). IR (KBr pellet): ν = 650.6, 775.9, 1090.0, 1213.0, 1607.5, 1730.5, 1783.1, 3259.7, 3435.3 cm^{-1}. HRMS (ESI-TOF): m/z calcd: 388.9520 $[M]^+$, found: 388.9518 $[M]^+$.

(4-Tetrathiafulvalenylmethoxyl)-N-propylacetamide (Model). (4-Tetrathiafulvalenylmethoxyl) acetic acid (100 mg, 0.34 mmol), EDC (130 mg, 0.68 mmol), and *N*-hydroxybenzotrizole (HOBt) (46 mg, 34

dx.doi.org/10.1021/la404349w | Langmuir 2014, 30, 718−726

mmol) were mixed in 10 mL dry THF. After the reaction mixture was stirred under nitrogen at room temperature for 30 min, propylamine (0.14 mL, 1.17 mmol) was added, and the mixture was reacted overnight. The solvent was removed under vacuum, and the residue was dissolved in CH_2Cl_2, was washed with water (three times), and then was dried with Mg_2SO_4. After evaporation of the solvent, the crude product was purified by column chromatography on silica gel (CH_2Cl_2/CH_3OH, 15:1, v/v), giving the product (101 mg, 86%) as a yellow solid. ^{1}H NMR (DMSO-d_6): δ = 6.76 (s, 1H), 6.72 (s, 2H), 4.32 (s, $-OCH_2-$, 2H), 3.85 (s, TTFCH_2-, 2H), 3.09−2.99 (m, $-NHCH_2-$, 2H), 1.48−1.34 (m, $-NHCH_2CH_2-$, 2H), 0.83 (t, $-CH_2CH_3$, 3H). IR (KBr pellet): ν = 642.1, 766.7, 1083.0, 1354.8, 1606.7, 1650.2, 2931.0, 3325.3, 3437.1 cm^{-1}. HRMS (ESI-TOF): m/z calcd: 332.9986 $[M]^+$, found: 332.9982 $[M]^+$, 355.9880 $[M + Na]^+$.

General Procedure for the Synthesis of G*n*-PAMAM-TTF. G*n*-PAMAM (n = 0−2) was dissolved in 1 mL CH_3OH and was added dropwise to a solution of succinimido-*N*-(4-tetrathiafulvalenylmethoxyl) acetate in 5 mL THF. The yellow solution was stirred under nitrogen at room temperature overnight. The solvent was removed under vacuum, and the residue was dissolved in DMSO and was precipitated in Et_2O to yield G*n*-PAMAM-TTF.

G0-PMAM-TTF. The product was synthesized according to the general procedure from succinimido-*N*-(4-tetrathiafulvalenylmethoxyl) acetate (290 mg, 0.75 mmol) and G0-PAMAM (80 mg, 0.15 mmol) and was obtained as a yellow solid (160 mg, 64%). ^{1}H NMR (DMSO-d_6): δ = 7.99−7.88 (m, $-CONH-$, 8H), 6.76 (s, 4H), 6.72 (s, 8H), 4.32 (s, $-OCH_2-$, 8H), 3.86 (s, TTFCH_2-, 8H), 3.16(t, $-NHCH_2-$, 16H), 2.64 (t, $-COCH_2CH_2-$, 8H), 2.43 (s, $-NCH_2-$, 4H), 2.20 (t, $-COCH_2-$, 8H). IR (KBr pellet): ν = 647.5, 772.8, 1122.5, 1350.7, 1544.0, 1662.4, 2833.5, 2943.4, 3068.7, 3310.0, 3412.9 cm^{-1}. MS (MALDI-TOF): m/z calcd: $[M]^+$ 1614.3, found: 1637.1 $[M + Na]^+$.

G1-PMAM-TTF. It was prepared from succinimido-*N*-(4-tetrathiafulvalenylmethoxyl) acetate (280 mg, 0.72 mmol) and G1-PAMAM (92 mg, 0.064 mmol) to give G1-PAMAM-TTF as a yellow solid (167 mg, 72%). ^{1}H NMR (DMSO-d_6) δ = 7.97−7.88 (m, $-CONH-$, 16H), 6.76 (s, 8H), 6.71 (s, 16H), 4.32 (s, $-OCH_2-$, 16H), 3.86 (s, TTFCH_2-, 16H), 3.14 (m, $-NHCH_2-$, 40H), 2.66 (t, $-COCH_2CH_2-$, 24H), 2.43 (s, $-NCH_2-$, 12H), 2.19 (t, $-COCH_2-$, 24H). IR (KBr pellet): ν = 656.8, 778.3, 1120.9, 1351.4, 1544.8, 1636.9, 2933.3, 3071.8, 3313.1, 3408.3 cm^{-1}. MS (MALDI-TOF): m/z calcd: 3625.1 $[M]^+$, found: 3647.6 $[M + Na]^+$.

G2-PMAM-TTF. G2-PAMAM-TTF was synthesized from succinimido-*N*-(4-tetrathiafulvalenylmethoxyl) acetate (310 mg, 0.79 mmol) and G2-PAMAM (120 mg, 0.037 mmol) to give it as a yellow solid (160 mg, 57%). ^{1}H NMR (DMSO-d_6): δ = 7.92 (m, $-CONH-$, 32H)6.75 (s, 16H), 6.71 (s, 32H), 4.31 (s, $-OCH_2-$, 32H), 3.86 (s, TTFCH_2-, 32H), 3.11 (m, $-NHCH_2-$, 88H), 2.65 (s, $-COCH_2CH_2-$, 56H), 2.42 (s, NCH_2-, 28H), 2.19 (s, $-COCH_2-$, 56H). IR (KBr pellet): ν = 658.4, 757.4, 1120.2, 1350.7, 1546.4, 1633.8, 2934.9, 3071.0, 3301.5, 3411.3 cm^{-1}. MALDI-TOF MS (m/z): calcd for M^+ 7646.6, failed to obtain the molecular ion peak.

Preparation of Nanodispersions of G*n*-PAMAM-TTF and Solution of Model. A solution of G*n*-PAMAM-TTF or Model in DMSO (50 μL, 0.25−10 mM) was mixed with 5 mL Milli-Q water. The mixture was shaken for 30 s, and the nanodispersions of G*n*-PAMAM-TTF and the solution of Model were ready.

Encapsulation of NR in Nanospheres of G2-PAMAM-TTF and Release of NR. A solution of the mixture of NR and G2-PAMAM-TTF with the mole ratio [NR]/[G2-PAMAM-TTF] of 0.5 in DMSO (50 μL, 1 mM) was mixed with 5 mL Milli-Q water and then was shaken for 30 s to give the NR-loaded nanosphere dispersion. The release of NR from the NR-loaded nanospheres derived from G2-PAMAM-TTF was achieved by shaking the sample with continuous orbital rotation at 100 cycle min^{-1}. The release amount of NR was examined by monitoring the change of the fluorescence intensity at 656 nm with excitation at 580 nm.

■ ASSOCIATED CONTENT

Ⓢ Supporting Information

Characterization data of the synthetic compounds and nanospheres, UV−vis, EPR, DLS and cryo-TEM data of reversible redox processes, and fluorescence spectra of NR release experiments. This information is available free of charge via the Internet at http://pubs.acs.org/.

■ AUTHOR INFORMATION

Corresponding Authors

*E-mail: yili@mail.ipc.ac.cn.
*E-mail: zengyi@mail.ipc.ac.cn.
*E-mail: gqyang@iccas.ac.cn.

Notes

The authors declare no competing financial interest.

■ ACKNOWLEDGMENTS

Financial support from the National Natural Science Foundation of China (Nos. 21073215, 21103210, 21173245, 21004072, 21002109, 21233011, and 21273258) and 973 Program (Nos. 2013CB834505, 2010CB934500, 2013CB834700) is gratefully acknowledged.

■ REFERENCES

(1) Soussan, E.; Cassel, S.; Blanzat, M.; Rico-Lattes, I. Drug Delivery by Soft Matter: Matrix and Vesicular Carriers. *Angew. Chem., Int. Ed.* **2009**, *48*, 274−288.

(2) Xu, H. P.; Cao, W.; Zhang, X. Selenium-Containing Polymers: Promising Biomaterials for Controlled Release and Enzyme Mimics. *Acc. Chem. Res.* **2013**, *46*, 1647−1658.

(3) Li, Y.; Du, W.; Sun, G.; Wooley, K. L. pH-Responsive Shell Cross-Linked Nanoparticles with Hydrolytically Labile Cross-Links. *Macromolecules* **2008**, *41*, 6605−6607.

(4) Zhao, Y. L.; Li, Z. X.; Kabehie, S.; Botros, Y. Y.; Stoddart, J. F.; Zink, J. I. pH-Operated Nanopistons on the Surfaces of Mesoporous Silica Nanoparticles. *J. Am. Chem. Soc.* **2010**, *132*, 13016−13025.

(5) Han, P.; Ma, N.; Ren, H. F.; Xu, H. P.; Li, Z. B.; Wang, Z. Q.; Zhang, X. Oxidation-Responsive Micelles Based on a Selenium-Containing Polymeric Superamphiphile. *Langmuir* **2010**, *26*, 14414−14418.

(6) Dan, K.; Pan, R.; Ghosh, S. Aggregation and pH Responsive Disassembly of a New Acid-Labile Surfactant Synthesized by Thiol-Acrylate Michael Addition Reaction. *Langmuir* **2011**, *27*, 612−617.

(7) Zou, Z.; He, D.; He, X.; Wang, K.; Yang, X.; Qing, Z.; Zhou, Q. Natural Gelatin Capped Mesoporous Silica Nanoparticles for Intracellular Acid-Triggered Drug Delivery. *Langmuir* **2013**, *29*, 12804−12810.

(8) Kim, J. K.; Lee, E.; Lim, Y. B.; Lee, M. Supramolecular Capsules with Gated Pores from an Amphiphilic Rod Assembly. *Angew. Chem., Int. Ed.* **2008**, *47*, 4662−4666.

(9) Aznar, E.; Mondragon, L.; Ros-Lis, J. V.; Sancenon, F.; Marcos, M. D.; Martinez-Manez, R.; Soto, J.; Perez-Paya, E.; Amoros, P. Finely Tuned Temperature-Controlled Cargo Release Using Paraffin-Capped Mesoporous Silica Nanoparticles. *Angew. Chem., Int. Ed.* **2011**, *50*, 11172−11175.

(10) Loh, X. J.; Tsai, M. H.; del Barrio, J.; Appel, E. A.; Lee, T. C.; Scherman, O. A. Triggered Insulin Release Studies of Triply Responsive Supramolecular Micelles. *Polym. Chem.* **2012**, *3*, 3180−3188.

(11) Chen, K. J.; Liang, H. F.; Chen, H. L.; Wang, Y. C.; Cheng, P. Y.; Liu, H. L.; Xia, Y. N.; Sung, H. W. A Thermoresponsive Bubble-Generating Liposomal System for Triggering Localized Extracellular Drug Delivery. *ACS Nano* **2013**, *7*, 438−446.

(12) Amir, R. J.; Zhong, S.; Pochan, D. J.; Hawker, C. J. Enzymatically Triggered Self-Assembly of Block Copolymers. *J. Am. Chem. Soc.* **2009**, *131*, 13949−13950.

(13) Azagarsamy, M. A.; Sokkalingam, P.; Thayumanavan, S. Enzyme-Triggered Disassembly of Dendrimer-Based Amphiphilic Nanocontainers. *J. Am. Chem. Soc.* **2009**, *131*, 14184−14185.
(14) Wang, C.; Chen, Q. S.; Wang, Z. Q.; Zhang, X. An Enzyme-Responsive Polymeric Superamphiphile. *Angew. Chem., Int. Ed.* **2010**, *49*, 8612−8615.
(15) Bernardos, A.; Mondragon, L.; Javakhishvili, I.; Mas, N.; de la Torre, C.; Martinez-Manez, R.; Sancenon, F.; Barat, J. M.; Hvilsted, S.; Orzaez, M.; Perez-Paya, E.; Amoros, P. Azobenzene Polyesters Used as Gate-Like Scaffolds in Nanoscopic Hybrid Systems. *Chem.—Eur. J.* **2012**, *18*, 13068−13078.
(16) Ong, W.; Yang, Y. M.; Cruciano, A. C.; McCarley, R. L. Redox-Triggered Contents Release from Liposomes. *J. Am. Chem. Soc.* **2008**, *130*, 14739−14744.
(17) Kim, E.; Kim, D.; Jung, H.; Lee, J.; Paul, S.; Selvapalam, N.; Yang, Y.; Lim, N.; Park, C. G.; Kim, K. Facile, Template-Free Synthesis of Stimuli-Responsive Polymer Nanocapsules for Targeted Drug Delivery. *Angew. Chem., Int. Ed.* **2010**, *49*, 4405−4408.
(18) Park, K. M.; Lee, D. W.; Sarkar, B.; Jung, H.; Kim, J.; Ko, Y. H.; Lee, K. E.; Jeon, H.; Kim, K. Reduction-Sensitive, Robust Vesicles with a Non-Covalently Modifiable Surface as a Multifunctional Drug-Delivery Platform. *Small* **2010**, *6*, 1430−1441.
(19) Zhang, S. Y.; Zhao, Y. Rapid Release of Entrapped Contents from Multi-Functionalizable, Surface Cross-Linked Micelles upon Different Stimulation. *J. Am. Chem. Soc.* **2010**, *132*, 10642−10644.
(20) Zhang, S. Y.; Zhao, Y. Controlled Release from Cleavable Polymerized Liposomes upon Redox and pH Stimulation. *Bioconjugate Chem.* **2011**, *22*, 523−528.
(21) Staff, R. H.; Gallei, M.; Mazurowski, M.; Rehahn, M.; Berger, R.; Landfester, K.; Crespy, D. Patchy Nanocapsules of Poly(vinylferrocene)-Based Block Copolymers for Redox-Responsive Release. *ACS Nano* **2012**, *6*, 9042−9049.
(22) Mynar, J. L.; Goodwin, A. P.; Cohen, J. A.; Ma, Y.; Fleming, G. R.; Frechet, J. M. J. Two-Photon Degradable Supramolecular Assemblies of Linear-Dendritic Copolymers. *Chem. Commun.* **2007**, 2081−2082.
(23) Babin, J.; Pelletier, M.; Lepage, M.; Allard, J. F.; Morris, D.; Zhao, Y. A New Two-Photon-Sensitive Block Copolymer Nanocarrier. *Angew. Chem., Int. Ed.* **2009**, *48*, 3329−3332.
(24) Wang, Y. P.; Han, P.; Xu, H. P.; Wang, Z. Q.; Zhang, X.; Kabanov, A. V. Photocontrolled Self-Assembly and Disassembly of Block Ionomer Complex Vesicles: A Facile Approach toward Supramolecular Polymer Nanocontainers. *Langmuir* **2010**, *26*, 709−715.
(25) Liu, Z. Z.; Lin, Q. N.; Huang, Q.; Liu, H.; Bao, C. Y.; Zhang, W. J.; Zhong, X. H.; Zhu, L. Y. Semiconductor Quantum Dots Photosensitizing Release of Anticancer Drug. *Chem. Commun.* **2011**, *47*, 1482−1484.
(26) Yesilyurt, V.; Ramireddy, R.; Thayumanavan, S. Photoregulated Release of Noncovalent Guests from Dendritic Amphiphilic Nanocontainers. *Angew. Chem., Int. Ed.* **2011**, *50*, 3038−3042.
(27) Zhao, Y. Light-Responsive Block Copolymer Micelles. *Macromolecules* **2012**, *45*, 3647−3657.
(28) Dong, J. M.; Zeng, Y.; Xun, Z. Q.; Han, Y. B.; Chen, J. P.; Li, Y. Y.; Li, Y. Stabilized Vesicles Consisting of Small Amphiphiles for Stepwise Photorelease via UV Light. *Langmuir* **2012**, *28*, 1733−1737.
(29) Dong, J. M.; Xun, Z. Q.; Zeng, Y.; Yu, T. J.; Han, Y. B.; Chen, J. P.; Li, Y. Y.; Yang, G. Q.; Li, Y. A Versatile and Robust Vesicle Based on a Photocleavable Surfactant for Two-Photon-Tuned Release. *Chem.—Eur. J.* **2013**, *19*, 7931−7936.
(30) Bigot, J.; Charleux, B.; Cooke, G.; Delattre, F.; Fournier, D.; Lyskawa, J.; Sambe, L.; Stoffelbach, F.; Woisel, P. Tetrathiafulvalene End-Functionalized Poly(*N*-isopropylacrylamide): A New Class of Amphiphilic Polymer for the Creation of Multistimuli Responsive Micelles. *J. Am. Chem. Soc.* **2010**, *132*, 10796−10801.
(31) Sambe, L.; Stoffelbach, F.; Lyskawa, J.; Delattre, F.; Fournier, D.; Bouteiller, L.; Charleux, B.; Cooke, G.; Woisel, P. Host-Guest Modulation of the Micellization of a Tetrathiafulvalene-Functionalized Poly(N-isopropylacrylamide). *Macromolecules* **2011**, *44*, 6532−6538.
(32) Loh, X. J.; del Barrio, J.; Toh, P. P. C.; Lee, T. C.; Jiao, D. Z.; Rauwald, U.; Appel, E. A.; Scherman, O. A. Triply Triggered Doxorubicin Release From Supramolecular Nanocontainers. *Biomacromolecules* **2012**, *13*, 84−91.
(33) Sun, Y. L.; Yang, B. J.; Zhang, S. X. A.; Yang, Y. W. Cucurbit[7]uril Pseudorotaxane-Based Photoresponsive Supramolecular Nanovalve. *Chem.—Eur. J.* **2012**, *18*, 9212−9216.
(34) Duan, Q. P.; Cao, Y.; Li, Y.; Hu, X. Y.; Xiao, T. X.; Lin, C.; Pan, Y.; Wang, L. Y. pH-Responsive Supramolecular Vesicles Based on Water-Soluble Pillar[6]arene and Ferrocene Derivative for Drug Delivery. *J. Am. Chem. Soc.* **2013**, *135*, 10542−10549.
(35) Patri, A. K.; Kukowska-Latallo, J. F.; Baker, J. R. Targeted Drug Delivery with Dendrimers: Comparison of the Release Kinetics of Covalently Conjugated Drug and Non-Covalent Drug Inclusion Complex. *Adv. Drug Delivery Rev.* **2005**, *57*, 2203−2214.
(36) Fox, M. E.; Szoka, F. C.; Frechet, J. M. J. Soluble Polymer Carriers for the Treatment of Cancer: The Importance of Molecular Architecture. *Acc. Chem. Res.* **2009**, *42*, 1141−1151.
(37) Tekade, R. K.; Kumar, P. V.; Jain, N. K. Dendrimers in Oncology: An Expanding Horizon. *Chem. Rev.* **2009**, *109*, 49−87.
(38) Sevenson, S.; Tomalia, D. A. Dendrimers in Biomedical Applications-Reflections on the Field. *Adv. Drug Delivery Rev.* **2012**, *64*, 102−115.
(39) Kitchens, K. M.; El-Sayed, M. E. H.; Ghandehari, H. Transepithelial and Endothelial Transport of Poly (amidoamine) Dendrimers. *Adv. Drug Delivery Rev.* **2005**, *57*, 2163−2176.
(40) Kolhatkar, R. B.; Kitchens, K. M.; Swaan, P. W.; Ghandehari, H. Surface Acetylation of Polyamidoamine (PAMAM) Dendrimers Decreases Cytotoxicity while Maintaining Membrane Permeability. *Bioconjugate Chem.* **2007**, *18*, 2054−2060.
(41) Moussodia, R. O.; Balan, L.; Merlin, C.; Mustin, C.; Schneider, R. Biocompatible and Stable ZnO Quantum Dots Generated by Functionalization with Siloxane-Core PAMAM Dendrons. *J. Mater. Chem.* **2010**, *20*, 1147−1155.
(42) Giffard, H.; Mabon, G.; Leclair, E.; Mercier, N.; Allain, M.; Gorgues, A.; Molinie, P.; Neilands, O.; Krief, P.; Khodorkovsky, V. Oxidation of TTF Derivatives Using (Diacetoxyiodo)benzene: A General Chemical Route toward Cation Radicals, Dications, and Nonstoichiometric Salts. *J. Am. Chem. Soc.* **2001**, *123*, 3852−3853.
(43) Chiang, P. T.; Chen, N. C.; Lai, C. C.; Chiu, S. H. Direct Observation of Mixed-Valence and Radical Cation Dimer States of Tetrathiafulvalene in Solution at Room Temperature: Association and Dissociation of Molecular Clip Dimers under Oxidative Control. *Chem.—Eur. J.* **2008**, *14*, 6546−6552.
(44) Spruell, J. M.; Coskun, A.; Friedman, D. C.; Forgan, R. S.; Sarjeant, A. A.; Trabolsi, A.; Fahrenbach, A. C.; Barin, G.; Paxton, W. F.; Dey, S. K.; Olson, M. A.; Benitez, D.; Tkatchouk, E.; Colvin, M. T.; Carmielli, R.; Caldwell, S. T.; Rosair, G. M.; Hewage, S. G.; Duclairoir, F.; Seymour, J. L.; Slawin, A. M. Z.; Goddard, W. A.; Wasielewski, M. R.; Cooke, G.; Stoddart, J. F. Highly Stable Tetrathiafulvalene Radical Dimers in [3]Catenanes. *Nat. Chem.* **2010**, *2*, 870−879.
(45) Wasielewski, M. R.; Coskun, A.; Spruell, J. M.; Barin, G.; Fahrenbach, A. C.; Forgan, R. S.; Colvin, M. T.; Carmieli, R.; Benitez, D.; Tkatchouk, E.; Friedman, D. C.; Sarjeant, A. A.; Goddard, W. A.; Stoddart, J. F. Mechanically Stabilized Tetrathiafulvalene Radical Dimers. *J. Am. Chem. Soc.* **2011**, *133*, 4538−4547.
(46) Kim, K.; Ziganshina, A. Y.; Ko, Y. H.; Jeon, W. S. Stable Pi-Dimer of a Tetrathiafulvalene Cation Radical Encapsulated in the Cavity of Cucurbit[8]uril. *Chem. Commun.* **2004**, 806−807.
(47) Zhang, Y. M.; Chen, Y.; Zhuang, R. J.; Liu, Y. Construction and Radical Cation Stabilisation of a Supramolecular Dyad by Tetrathiafulvalene-Modified-Cyclodextrin and Cucurbit[7]uril. *Supramol. Chem.* **2011**, *23*, 372−378.
(48) Hwang, I.; Ziganshina, A. Y.; Ko, Y. H.; Yun, G.; Kim, K. A New Three-Way Supramolecular Switch Based on Redox-Controlled Interconversion of Hetero- and Homo-Guest-Pair Inclusion Inside a Host Molecule. *Chem. Commun.* **2009**, 416−418.
(49) Kim, J.; Jung, I. S.; Kim, S. Y.; Lee, E.; Kang, J. K.; Sakamoto, S.; Yamaguchi, K.; Kim, K. New Cucurbituril Homologues: Syntheses,

Isolation, Characterization, and X-ray Crystal Structures of Cucurbit-[*n*]uril (*n* = 5, 7, and 8). *J. Am. Chem. Soc.* **2000**, *122*, 540−541.
(50) Lee, J. W.; Samal, S.; Selvapalam, N.; Kim, H. J.; Kim, K. Cucurbituril Homologues and Derivatives: New Opportunities in Supramolecular Chemistry. *Acc. Chem. Res.* **2003**, *36*, 621−630.
(51) Lagona, J.; Mukhopadhyay, P.; Chakrabarti, S.; Isaacs, L. The Cucurbit[n]uril Family. *Angew. Chem., Int. Ed.* **2005**, *44*, 4844−4870.
(52) Isaacs, L.; Liu, S. M.; Ruspic, C.; Mukhopadhyay, P.; Chakrabarti, S.; Zavalij, P. Y. The Cucurbit[n]uril Family: Prime Components for Self-Sorting Systems. *J. Am. Chem. Soc.* **2005**, *127*, 15959−15967.
(53) Zeng, Y.; Li, Y. Y.; Li, M.; Yang, G. Q.; Li, Y. Enhancement of Energy Utilization in Light-Harvesting Dendrimers by the Pseudorotaxane Formation at Periphery. *J. Am. Chem. Soc.* **2009**, *131*, 9100−9106.
(54) Wang, C.; Dyar, S. M.; Cao, D.; Fahrenbach, A. C.; Horwitz, N.; Colvin, M. T.; Carmieli, R.; Stern, C. L.; Dey, S. K.; Wasielewski, M. R.; Stoddart, J. F. Tetrathiafulvalene Hetero Radical Cation Dimerization in a Redox-Active [2]Catenane. *J. Am. Chem. Soc.* **2012**, *134*, 19136−19145.
(55) Melby, L. R.; Hartzler, H. D.; Sheppard, W. A. Improved Synthesis of Tetrathiafulvalene. *J. Org. Chem.* **1974**, *39*, 2456−2458.
(56) Wudl, F.; Kaplan, M. L.; Hufnagel, E. J.; Southwic, Ew Convenient Synthesis of 1,4,5,8-Tetrahydro-1,4,5,8-Tetrathiafulvalene. *J. Org. Chem.* **1974**, *39*, 3608−3609.
(57) Garin, J.; Orduna, J.; Uriel, S.; Moore, A. J.; Bryce, M. R.; Wegener, S.; Yufit, D. S.; Howard, J. A. K. Improved Syntheses of Carboxytetrathiafulvalene, Formyltetrathiafulvalene and (Hydroxymethyl)Tetrathiafulvalene - Versatile Building-Blocks for New Functionalized Tetrathiafulvalene Derivatives. *Synthesis-Stuttgart* **1994**, 489−493.
(58) Kitamura, T.; Nakaso, S.; Mizoshita, N.; Tochigi, Y.; Shimomura, T.; Moriyama, M.; Ito, K.; Kato, T. Electroactive Supramolecular Self-Assembled Fibers Comprised of Doped Tetrathiafulvalene-Based Gelators. *J. Am. Chem. Soc.* **2005**, *127*, 14769−14775.